COBEM 2023 27TH INTERNATIONAL CONGRESS OF MECHANICAL ENGENEERING

ABCM Brazilian Society of Mechanical Sciences and Engineering
27th ABCM International Congress of Mechanical Engineering
December 04-08, 2023, Florianópolis-SC, Brazil

COB-2023-2422
EXPERIMENTAL DETERMINATION OF ADDED MASSES FOR AN OPEN FRAME ROV USED IN THE STOCK ASSESSMENT OF SCALLOPS

Paola Andrea Fonseca Florez
Universidade Federal do ABC
paola.fonseca@ufabc.edu.br

Juan Pablo Julca Avila
Universidade Federal do ABC
juan.avila@ufabc.edu.br

Abstract. *The main objective of this work is to determine the added masses in surge, sway, and heave directions of an open-frame ROV used for the stock assessment of scallops on the Peruvian coast. The method consisted of supporting a 1:3 scale model of the prototype through springs and making it oscillate freely in still water with different amplitudes and frequencies. The Reynolds Number (Re) of the tests were in a range of $0.14\times10^5 \leq Re \leq 0.67\times10^5$. The acceleration of the model vibrating freely and damply in water was measured experimentally. The added mass in one motion direction was determined using the damped natural frequency equation for a system mass-spring-damper of 1-DOF. The results demonstrated that for Keulegan–Carpenter numbers (KC) in the range of $1.52 \leq KC \leq 3.43$, the added mass values were similars between them for the heave direction, there was no significant variation of the added masses within the frequencies and amplitudes imposed in the tests. In naval and oceanic engineering, the added mass of a body moving in water is usually determined using the simplified form of the damped natural frequency equation, where the damping effects are not considered. However, this work suggests that the simplified form can be used with good accuracy for $KC \leq 0.46$, but for $KC \geq 1.52$ must be used the exact form of the equation because the damping effects influence more and more by increasing KC.*

Keywords: *Added mass, underwater vehicle, free vibration test, damping effects.*

1. INTRODUCTION

The group of researchers in the Company Veox from Peru is developing a ROV (remotely operated vehicle) called Hindrax for the stock assessment of scallop production on the Peruvian coast, which is described in Huamani *et al.* (2023). The role of the vehicle is to take videos of the scallops on the seabed using a high-resolution camera on board the vehicle. The image processing algorithms of the Hindrax ROV can estimate the number and size of scallops per unit area as long as the videos are stable and there is a constant separation distance between the vehicle and the seabed. However, some disturbances can affect vehicle operation, such as ocean currents and the irregularities of the ocean floor. The latter is a disturbance because it influences the altitude control system. Therefore, the control system in the surge, sway, and heave directions should be based on the mathematical model and the knowledge of the hydrodynamic parameters that compose it.

The added mass is a hydrodynamic parameter that quantifies fluid inertia, which affects vehicle motion when it accelerates through a fluid. It can be experimental and numerically determined. If the body has an irregular shape, the added mass numerical determination is more complicated, and the results are inaccurate.

In Brooks (1976), the added mass of different propellers and a disk were experimentally determined, and a theory was proposed to determine it, too. The experimental tests consisted of submerging the body, supporting it with two cantilever strips, and generating a perturbation that allowed it to oscillate free and vertically. An accelerometer was attached to the system to measure the fundamental vibration frequency with the submerged propeller. Then, the same test was made in the air, but a lumped mass was attached to the system. This mass allowed it to oscillate in the air with the same frequency at which the propeller oscillated when it was submerged in water. Therefore, the added mass was equal to the lumped mass attached to the air oscillations. The experimental result were compared with the theory proposed that consisted of determining the added mass solving Laplace's equation subject to no normal inflow to the propeller surface. A disagreement between the proposed theory and experimental results was shown. The theoretical results had a relative error concerning the experimental data obtained for propellers of 15% to 30%, and for the disk, the error was within 2%. It assumed that the errors were caused by the vorticity in the propellers' leading and trailing edges. The magnitude of the forces caused by the vorticity could not be predicted at that time.

Stelson and Mavis (1957) determined the added mass based on the same experiments that Brooks (1976). The body

was supported by a rod attached to a beam that contained a magnet. With the system vibration, the magnet produced a potential in a surrounding coil. An oscillograph measured the varying potential to obtain the fundamental vibration frequency. The bodies tested had simple shapes and, the experimental and theory results were coherent.

The application of the model mass-spring for 1-DOF of vibration provides a practical method for calculating added masses. Hamilton (1997) used this method to determine the added mass of ocean moorings. The experiment was made from a ship by releasing all elements that made part of the mooring in the sea. First, the float elements were deployed, and then the anchor was released. The tension variation of the mooring was measured once the anchor achieved the seabed; the tension records let us know the natural frequency and demonstrated that the system was under-damped. The equivalent stiffness of the system was already known. In that way, the added mass was calculated by the equation of undamped natural frequency.

The added mass was determined in a scaled model of a ROV in Avila *et al.* (2005) using the mass-spring equation of free vibration in 1-DOF. The experimental setup consisted of holding the model with eight springs submerged in water and generating a disturbance that made it vibrate on one axis. The acceleration model was measured with an accelerometer that allowed it to obtain the natural frequency, then the added mass was estimated from the equation of the undamped natural frequency. The same procedure was used in Felix (2013) to determine the added mass of an offshore floating platform using its reduced model. It was submerged in a water tank with a mass of 150 kg, then the mass was removed, and the model began to oscillate on the surface. The displacement signal in the oscillation was measured with an ultrasonic sensor to determine the added mass, neglecting the damping effects.

In You *et al.* (2013) proposed a free decay method based on a pendulum motion to determine the added mass of a reduced scale model ROV. The model was attached to the end of a rod. Then, the rod performed a free decay oscillatory motion in the water, and the trajectory of the pendulum motion was captured by a camera, which led it to determine the added mass parameter from the pendulum motion equation. This parameter was also determined using the fluid dynamic software Wamit, and the accuracy of results obtained using the software was within 2% to 19% less than the experimental results.

In Cely *et al.* (2019), two experimental methods to determine the added mass of a ROV were compared: the free decomposition test based on a mass-spring system, similar to the one used by Avila *et al.* (2005), and the tests based on the motion of a pendulum. The latter consisted of measuring the angular position of the ROV during the six launches from different initial angles and applying the least square method and Morison's equation using the position data collected in the launches to obtain the drag coefficients and added masses. The results of added masses obtained in the free decay tests based on the pendulum's motion had a relative error concerning the results obtained with the tests with springs between 10% and 28%. The authors in this paper attributed the error to the spring method, which did not require the method of least squares to solve it, and to nonlinear behavior in the free decay pendulum test because the response had variations when the initial angle was greater.

A submerged body in water can oscillate using a PMM (planar motion mechanism) to determine its drag coefficients and added masses. This experiment was conducted by Avila (2008), where a ROV attached to a PMM that oscillated in different amplitudes and periods. The GLS (generalized least squares) method was used to calculate the drag and inertia coefficients from the force and velocity measurements. However, using PMM is expensive and difficult to implement in the design stage before manufacturing the final prototype.

The numerical determination of the hydrodynamic parameters is important in the preliminary stages of the design of a ROV. In Hammoud *et al.* (2021), a free oscillation study of a ROV held by springs submerged in water was done using the software COMSOL Multiphysics. Compared with the potential theory described by Sahili *et al.* (2018), the theory results presented a relative error between 8% and 17% regarding the results obtained using the software COMSOL Multiphysics. The difference was because the potential theory neglected the viscous effects.

The main objective of this work is to determine the added masses of a ROV used for the stock assessment of Peruvian scallops. The added mass determination is crucial to the motion control of the vehicle, especially to its altitude control. The method used in this work to determine the added masses is economical and can be done in the vehicle design stage. The experiments were based on free oscillation tests using springs and the reduced scale model of the ROV to obtain the added masses in the surge, sway, and heave directions. The previous authors determined the added masses from the equation of undamped natural frequency but this work determines them using damped and undamped natural frequency equations, and then the added masses obtained from both equations are compared.

2. Mechanical design and sensory system

The Hindrax ROV is an underwater vehicle, classified as open-frame, and it is shown in Figure 1a. The vehicle's main frame is made of acrylic plates and, the structural joints and supports for both pressure vessels and thrusters are made of PETG (polyethylene terephthalate glycol) and fabricated using a 3D printer (see Figure 1a). The upper part of the vehicle has two thin-walled tubes that work as floats and a pressure vessel made of acrylic that contains the control electronics. The bottom part of the vehicle consists of a pressure vessel for the battery and two PETG tubes containing the ballasts. The vehicle size is 0.59 m, 0.47 m, and 0.4 m in length, width, and height, respectively. It has positive buoyancy with a

(a) (b)

Figure 1: (a) The Hindrax ROV prototype. (b) The Hindrax ROV model reduced on a scale of 1:3

force of 0.83 N, which means the vehicle floats when its thrusters are turned off. The total mass of the Hindrax ROV is 15.22 kg, and its volume, 0.0153 m^3. The Hindrax ROV has eight thrusters that let it move in 6-DOF. They are divided into two layers: four thrusters at the top layout provide power for the heave, roll, and pitch motion, and the remaining thrusters at the bottom layout allow the motion in the surge, sway, and yaw motion as Figure 2 illustrates.

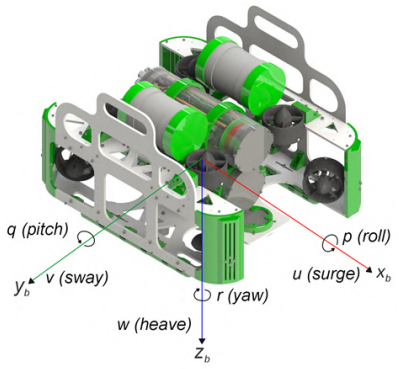

Figure 2: Local reference frame and DOFs of the Hindrax ROV.

Figure 1b shows the Hindrax ROV reduced-scale model. It was fabricated with a 3D printer using PLA (polylactic acid) on a scale of 1:3. The model has 0.19 m, 0.15 m, and 0.13 in length, width, and height, respectively, total mass, 0.39 kg, and volume, 0.00056 m^3.

Table 1: Hindrax sensors description

Variable	**Sensor**	**Communitation**	**Precision**
Velocity (surge and sway)	DVL-75(Cerulean)	Serial	Mean error: 5% of distance traveled
Angular velocities and heading	Gyroscopes and the magnetometer in the DVL-75(Cerulean)	Serial	Depends on its calibration
Accelerations (x ,y and z)	Acelerometer(ICM-20948)	I2C	Full scale range of ±2 , ±4 g, ± 8g, and ±16 g
Angular velocities	Gyroscope(ICM-20948)	I2C	Full-scale range of ±250 dps, ±500 dps, ±1000 dps, and ±2000 dps
Heading	Magnetometer(ICM-20948)	I2C	Wide range to ±4900 µT
Depth	Pressure(MS5837)	I2C	± 0.007 PSI
Altitude	Sonar(BlueRobotics)	Serial	Resolution of 0.5%

The vehicle sensory system is described in Table 1. This system is composed of a sonar that measures the altitude; the

inertial unit IMU contains accelerometers, gyroscopes, and a magnetometer to know the accelerations, angular velocities, and heading, respectively. The Doppler effect sensor DVL measures the velocities in the surge and sway directions; it can not measure the velocity in the heave direction. This sensor also contains gyroscopes and a magnetometer to measure angular velocities and heading. Finally, a pressure sensor is used to measure the depth.

3. Mathematical model

The free vibration of the body submerged in water is modeled by the equation of 1-DOF damped free vibration of a system consisting of a mass, a mass-less spring and a damper, as shown in Figure 3.

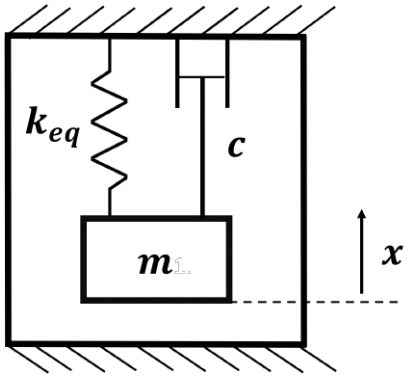

Figure 3: Equivalent model of damped free vibration in 1-DOF of a body.

Let m_b be the mass of the body and m_{ad} the added mass, the total mass of the system $m = m_b + m_{ad}$. The equivalent stiffness of the system is k_{eq}, and the damping coefficient c.White (2004) describes the parameter m_{ad} as the finite fluid mass pushed out of the way when a body moves through a fluid. If the body is accelerated, the surrounding fluid must also be accelerated; the amount of mass accelerated is the added mass.

The system vibrates around its equilibrium position. If the displacement of the system is described by the position coordinate x, the equation of free vibration is given by Summer and Fredsoe (2006),

$$m\ddot{x} + c\dot{x} + k_{eq}x = 0, \tag{1}$$

where the first term on the left side is the inertial force due to the total mass of the system, $\ddot{x}$ being the body's acceleration. The second term is the damping force due to the viscosity of the fluid, $\dot{x}$ being the body's velocity,and the third term is the elastic force of the springs.

The response of the system is characterized by the damped natural frequency ω_d,

$$\omega_d = \omega_n(1-\zeta^2)^{1/2}, \tag{2}$$

where ω_n is the undamped natural frequency and ζ, the damping ratio. This latter is defined by the logarithmic decrement δ of two consecutive peak amplitudes, x_1 and x_2 (see Figure 6b),

$$\delta = \ln\frac{x_1}{x_2} = \frac{2\pi\zeta}{\sqrt{1-\zeta^2}}. \tag{3}$$

As x_1 and x_2 are measured experimentally, then δ is calculated from Eq. (3). Knowing δ, Eq. (3) also is used to determine ζ.

The undamped natural frequency ω_n is defined as,

$$\omega_n = \sqrt{\frac{k_{eq}}{m}} = \sqrt{\frac{k_{eq}}{m_b + m_{ad}}}. \tag{4}$$

If k_{eq} is measured experimentally in the springs, ω_d is determined from the displacement signal of the free vibration system, ζ is calculated using Eq. (3) as was previously explained, and m_b is known, then is possible to obtain an expression to calculate m_{ad} substituting Eq. (4) in Eq. (2) as,

$$m_{ad} = \frac{k_{eq}(1-\zeta^2)}{\omega_d^2} - m_b \tag{5}$$

and, the damping coefficient c is defined in the equation of free vibration as,

$$c = 2\zeta\sqrt{k_{eq}(m_b + m_{ad})}. \tag{6}$$

If we omit the damping effects the added mass is determined using Eq. (4) as,

$$m_{ad} = \frac{k_{eq}}{\omega_n^2} - m_b \tag{7}$$

Once m_{ad} was determined, the inertia coefficient C_M is calculated as,

$$C_M = \frac{m_{ad}}{\rho \forall}, \tag{8}$$

where ρ is the fluid density and $\forall$, the volume of fluid displaced by the body.

The Keulegan-Carpenter number KC is a dimensionless parameter used in fluid dynamics to determine the relative contribution between the inertia and drag forces of a body exposed to an oscillatory flow. In the case of cylinders, it is given by Summer and Fredsoe (2006),

$$KC = \frac{2\pi A}{D}, \tag{9}$$

where D is the cylinder diameter and A, the oscillation amplitude. For cylinders, the characteristic length is its diameter, however, for the scaled model, the characteristic length is based on the volume of the model $\forall$, and is given by $\forall^{1/3}$. In this work, the parameter A to calculate KC is selected as initial displacement of the free vibration of the reduced scale model.

4. Experimental tests

The experimental assembly that determined the added masses of the scaled model is shown in Figure 4. The model was supported by eight springs in a structure fabricated of wood with dimensions of 0.17 m, 0.4 m, and 0.35 m in length, width, and height, respectively.

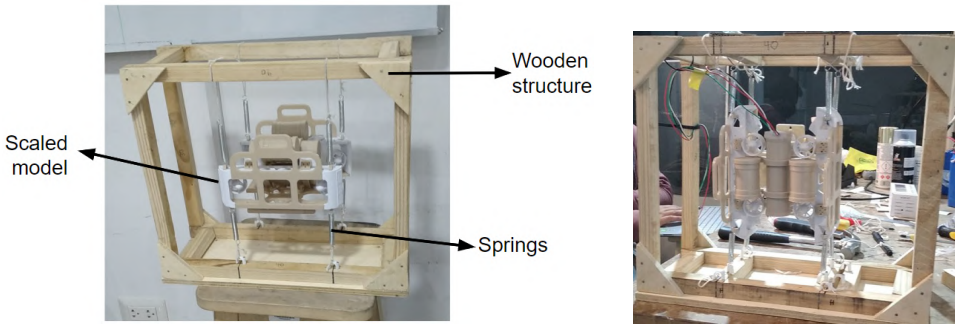

(a) (b)

Figure 4: Reduced model of the Hindrax ROV at 1:3 scale supported by springs to determine the added mass: Tests in (a) heave and (b) surge.

The wood structure allowed us to support the model with the springs arranged in the surge, sway, and heave directions. See Figure 2 for the local reference frame and the DOFs of the Hindrax ROV. The tests consisted of putting the structure shown in Figure 4 in still water with the model oriented in its direction to be tested, displacing the model up to a known position, and releasing it. The model started to oscillate in 1-DOF, and its acceleration was measured using an accelerometer by a period of 10 seconds.

The experimental setup is shown in Figure 5. The inertial sensor ICM-20948 described in Table 1, classified as a Micro-Mechanical System (MEMS), was fixed in the model with silicone. The acceleration data was acquired with a sampling rate of 330 Hz using the STF401R3 microcontroller. Then, the acceleration signal was sent to a PC via a serial protocol for its processing in MATLAB.

The initial displacement A at which the model was released is defined by the oscillation amplitude that the vehicle's prototype experiments in its operation. To do this, the following equation is used,

$$\left(\frac{A}{\forall^{1/3}}\right)_{prototype} = \left(\frac{A}{\forall^{1/3}}\right)_{model}, \tag{10}$$

where $\forall$ is the body volume and, $\forall^{1/3}$ its characteristic length. For the model, $\forall^{1/3}$ = 0.0824 m, and for the prototype, $\forall^{1/3}$ =0.2483 m.

The free oscillation tests were made with two spring groups of different equivalent stiffness. The equivalent stiffness of each spring group was calculated as follows: first, the stiffness of one unique spring was experimentally measured

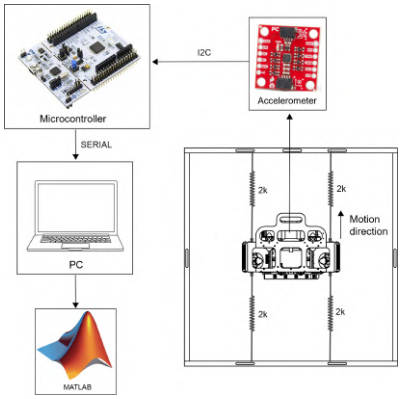

Figure 5: Experimental setup used for free oscillations tests.

by applying different forces at the end of it and measuring its elongations; after, since all eight springs were identical and distributed in parallel, the equivalent stiffness of the spring groups was obtained by multiplying the stiffness of one spring by eight. The stiffness of the springs was considered to be the same in the water and air. The equivalent stiffnesses obtained were 1127.7 N/m and 659.9 N/m; the first and last correspond to the spring groups of high and low equivalent stiffness.

Table 2 shows the equivalent stiffnesses, the initial displacements at which the model was released, and the oscillation amplitudes of the prototype. This latter was used to determine the initial displacements of the model using Eq. (10). The oscillation amplitude values of the vehicle were determined from its typical motions during the stock assessment of scallops, where for the surge and sway motions, the oscillation amplitudes were smaller than heave motion. The altitude control system of the Hindrax ROV keeps constant the separation distance between the prototype and the ocean floor. When the vehicle is moving in the surge and sway directions, the altitude control will make it oscillate in the heave direction due to the irregularities of the ocean floor, and the typical oscillation amplitudes in heave are shown in the last column of Table 2. Different initial displacements and two levels of equivalent stiffness, high and low, were considered for testing the oscillation amplitudes in heave.

Table 2: Experimental parameters for free oscillation tests.

Direction	k_{eq} (N/m)	A_{model} (mm)	$A_{prototype}$ (mm)
Surge	1127.7	4	12
Sway	1127.7	5	15
Heave	1127.7	6; 20; 25	18 ; 60 ; 75
	659.9	20; 25; 30; 35; 40; 45	60; 75; 90; 105; 120; 135

Figures 6a and 6b show, respectively, the experimentally measured acceleration and displacement signals for the test in the heave direction with an initial displacement of 20 mm. The displacement signal was calculated as the double integration of the acceleration signal.

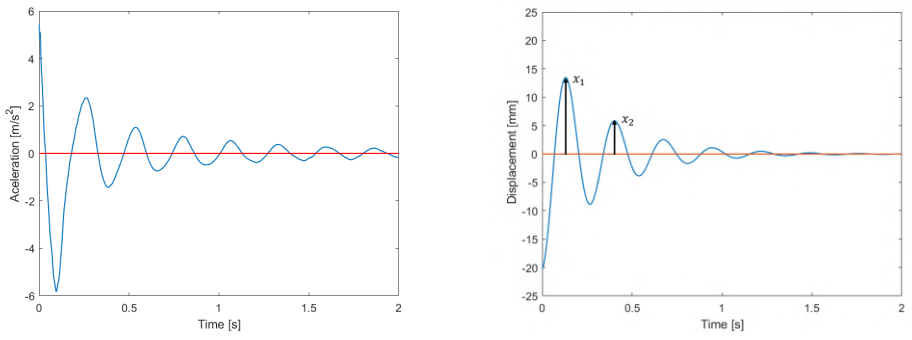

(a) (b)

Figure 6: (a) Acceleration signal and (b) displacement signal for the model during a free oscillation test in heave with an initial displacement of 20 mm.

The tests were made in a Reynolds Number range of $0.14\times10^5 \leq Re \leq 0.67\times10^5$. The Re is defined as $Re = \frac{U_m \forall^{1/3}}{\nu}$ where U_m is the maximum velocity achieved during the oscillations, ν is the kinematic viscosity of the water equal to $1.01 \times 10^{-6}\ m^2/s$, and $\forall^{1/3}$, the characteristic length of the model, previously defined.

5. Results and discussions

Results from free oscillation tests in the surge and sway directions are shown in Table 3. Tables 4 and 5 show the results obtained for heave direction with the spring groups of high and low equivalent stiffness, respectively.

Table 3: Experimental results for the surge and sway directions.

Direction	Initial displacement A (mm)	Damped frequency ω_d (rad/s)	Damping ratio ζ	Damping coefficient c (N.m.s)	m_{ad} based on ω_n (kg)	m_{ad} based on ω_d (kg)	Error	KC
Surge	4	36.7824	0.0713	4.35	0.4435	0.4401	0.77%	0.3
Sway	5	31.7580	0.1155	8.14	0.7281	0.7132	2.09%	0.38

Table 4: Tests results in the heave direction for the spring group of high equivalent stiffness, k_{eq} = 1127.7 N/m.

Direction	Initial displacement A (mm)	Damped frequency ω_d (rad/s)	Damping ratio ζ	Damping coefficient c (N.m.s)	m_{ad} based on ω_n (kg)	m_{ad} based on ω_d (kg)	Error	KC
Heave	6	30.3976	0.0604	4.47	0.8304	0.8260	0.53%	0.46
	20	30.1326	0.1154	8.56	0.8454	0.8289	1.99%	1.52
	25	29.966	0.172	12.75	0.8658	0.8287	4.48%	1.9

Table 5: Tests results in the heave direction for the spring group of low equivalent stiffness, k_{eq} = 659.9 N/m.

Direction	Initial displacement A (mm)	Damped frequency ω_d (rad/s)	Damping ratio ζ	Damping coefficient c (N.m.s)	m_{ad} based on ω_n (kg)	m_{ad} based on ω_d (kg)	Error	KC
Heave	20	23.1477	0.1328	7.57	0.8416	0.8198	2.66%	1.52
	25	23.0504	0.1656	9.48	0.8520	0.8179	4.17%	1.9
	30	23.0629	0.1518	8.69	0.8506	0.8220	3.48%	2.28
	35	22.9846	0.1702	9.77	0.8591	0.8229	4.4%	2.66
	40	23.0505	0.1613	9.23	0.852	0.8197	3.94%	3.05
	45	22.8966	0.1992	11.48	0.8687	0.8187	6.1%	3.43

For the Tables 3, 4 and 5, the second column contains the imposed initial displacement, A; the third column, the damped natural frequency, ω_d extracted from the displacement signals and using Eq. (2); the fourth and the fifth column presents the damping ratio ζ and the damping coefficient c, which are obtained from Eqs. (3) and (6), respectively; the sixth and seventh columns correspond to the added masses m_{ad} calculated using Eqs. (7) and (5), respectively; the penultimate column shows the relative error obtained by determining m_{ad} using Eq. (7) and based on ω_n instead of Eq. (5), which considers ω_d, being the m_{ad} value obtained with the latter equation used as a reference for error calculation. Equation. (11) was used to calculate this error. Finally, the last column contains the KC number, calculated using Eq. (9).

$$\%Error = \frac{(m_{ad})_{\omega_n} - (m_{ad})_{\omega_d}}{(m_{ad})_{\omega_d}} \times 100. \tag{11}$$

The added masses for the heave direction obtained based on ω_d from the tests made with different initial displacements and equivalent stiffnesses do not vary significantly between them. It is demonstrated by calculating the mean and the standard deviation of the added mass values given in the seventh column of Tables 4 and 5. The mean was 0.8227, and the standard deviation was $\pm$0.0042. The latter expressed in relative percentage is equal to 0.51%.

Observing Tables 4 and 5, it is noted that the errors increased with the initial displacement, A, and the KC number. The damping ratio ζ also increased when the model was released from higher initial displacement. Figures 7a and 7b

show the response of the model for initial displacements of 6 mm and 25 mm in the heave direction. Figure 7b shows a logarithmic decrement δ higher than Figure 7a because the distance traveled by the model was greater, leading to a higher velocity, increasing the influence of the drag force and the relative error in determining the added mass without the damping effects.

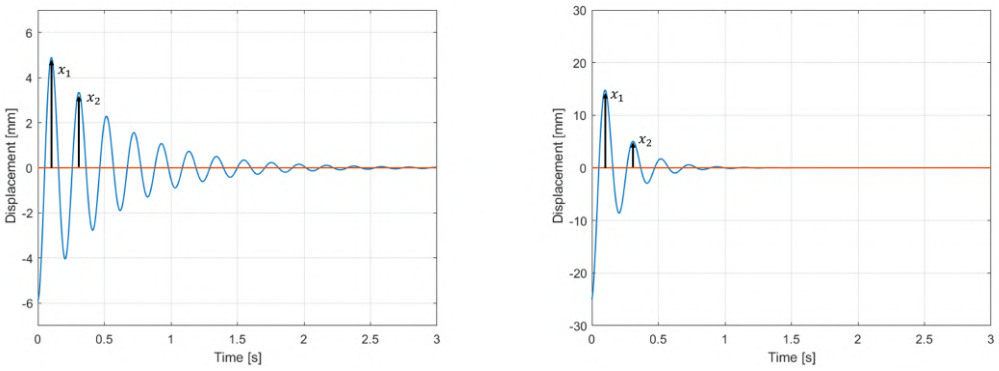

(a) (b)

Figure 7: Displacement signals in the heave direction obtained with the spring group of high equivalent stiffness: (a) initial displacement of 6 mm; (b) initial displacement, 25 mm.

According to Blevins (2001), a system is lightly damped when the damping ratio $\zeta \leq 0.05$; based on this, the response of the tests in heave are not classified as lightly damped due to the values of ζ in the fourth column in Tables 4 and 5 are between 0.06 to 0.19. The added masses obtained based on ω_d are almost the same within the damping ratios range, but those obtained based on ω_n are higher because the damping forces were not considered. In addition to that, it is observed that the difference between the added mass values obtained based on ω_n and ω_d increases with ζ.

Table 6: Added masses of the Hindrax ROV.

Direction	C_M	$m_{ad,prototype}$ based on ω_d (kg)
Surge	0.79	12.08
Sway	1.27	19.43
Heave	1.4692 ± 0.0075	22.48

Table 6 shows the inertia coefficients C_M and added masses m_{ad} of the Hindrax ROV prototype obtained from the tests in the surge, sway, and heave directions using the reduced model. All added masses from Table 6 were determined based on ω_d. C_M was calculated using Eq. (8) and the added mass values listed in the seventh column of Tables 3, 4 and 5. For heave, C_M and its standard deviation are calculated based on the mean value of all added mass obtained. With this information, the added masses of the Hindrax ROV prototype were calculated using the following equation,

$$m_{ad,prototype} = C_M \rho \forall_{prototype} \tag{12}$$

Where ρ is the water density equal to 1000 kg/m^3 and $\forall$, the volume of water displaced by the prototype equal to 0.0153 m^3, as was previously defined.

Table 7 shows a comparison of the results obtained in this work with the results of other researchers that also experimentally determined the C_M for other open frame ROVs, which have similar shapes to the Hindrax ROV, with 8 or 6 thrusters, two pressure vessels and a frame to support all the parts together. It is found that the results are coherent. It is especially noted that the C_M in the surge direction for the vehicle of Cely *et al.* (2019) and the Hindrax ROV have similar values equal to 0.82 and 0.79, respectively. These C_M are close to each other because the projected area of both vehicles for the surge direction has a similar geometry due to their pressure vessels are parallel to the vehicle's longitudinal direction.

Stuart and Woodgate (1955) made free decay tests based on the pendulum motion of cylinders submerged in water and measured the drag force during the oscillations; for the tests where $KC \leq 0.6$, was found that the logarithmic decrement did not vary significantly, suggesting that the regime flow in those conditions was viscous and laminar. On the other hand, Sarpkaya (1986), in their experimental studies of flow visualization with cylinders, noticed that for $1.1 \leq KC \leq 4$, the flow started to separate, appearing a pair of symmetric vortices and the flow was no longer laminar. In the present work, the tests in the heave direction were done with initial displacements between 6 mm and 45 mm and, KC in the range of

0.46 to 3.43. Those observations allow us to assume that the flow in the tests was not laminar and that there was vortex shedding for the initial displacements tested.

Table 7: Comparison of added masses obtained by different researchers.

ROV	Surge/Sway/Heave C_M	Kind of experiment	Sensor	Vehicle volume, m^3 / mass, kg
Avila *et al.* (2005)	0.43/0.67/1.32	Free oscillations with springs	Accelerometer	0.0236 /22.2
Cely *et al.* (2019)	0.82/0.19/1.16	Free oscillations with springs	Position transducer	3.44$\times$ 10^{-5} / 0.97
You *et al.* (2013)	0.58/1.49/3.07	Free oscillations based on pendulum motion	Cameras	Unregistered / 115
Hindrax ROV	0.79/1.27/1.48	Free oscillations based on pendulum motion	Accelerometer	56$\times 10^{-3}$/0.39

The added mass values obtained basing on ω_d for heave direction within the range 1.52$\leq KC \leq$ 3.43, see the seventh column in Tables 4 and 5, are similars one with each other because the flow regime is the same in all tests, being not laminar and with a slight shedding of symmetrical vortices according to Sarpkaya (1986). The damping force increases with KC; it is verified by seeing that the damping coefficient c, shown in the fifth column, increases with the KC value.

Making a comparison of the added masses obtained basing on ω_d and those obtained basing on ω_n, which are respectively, shown in columns seventh and sixth in Tables 4 and 5, this last is higher in all initial displacements tested because the equation to determine m_{ad} using ω_n, Eq. (7), does not consider the viscous damping effects.

The KC values shown in the last column of Tables 4 and 5 demonstrate that when KC is less than 0.46, the error of obtaining the added mass based on ω_n is less than 2%, but for KC values within the range 1.52$\leq KC \leq$ 3.43, the error is between 1.99% and 6.1%. Therefore, the formula for the added mass basing on ω_n, Eq. (7), when KC is less than 0.46, allows us to obtain results with more accuracy. However, for KC higher than 1.52, it is preferable to use the formula based on ω_d, Eq. (5), that is the exact equation for the added mass.

6. Conclusions

The added masses and inertia coefficients in surge, sway, and heave directions of a ROV for the stock assessment of scallops were determined through free oscillation tests in 1-DOF using a reduced scale model of the prototype submerged in water. The experiments in the heave direction were made using different initial displacements and two spring groups that let the model to oscillate with two different natural frequencies. The displacement signal during the oscillations of the model allows us to determine the damped natural frequency ω_d and the damping ratio ζ, being possible to calculate the added mass from Eq. (5) to each motion direction.

For the heave DOF, with both equivalent stiffnesses tested, the high of 1127 N/m and the low of 659 N/m, and oscillation amplitudes between 20 mm and 45 mm was found that the added masses obtained basing on ω_d, are practically the same with a dispersion of 0.52%. This similarity is attributed to the fact that the flow patterns are almost identical in the tests developed. The KC obtained in those tests is between 1.52 and 3.43, and according to Sarpkaya (1986), the flow presents a slight shedding of symmetrical vortices and is not laminar.

The error of calculating the added mass using Eq. (7) instead of Eq. (5) for 0.46$\leq KC \leq$ 3.43 in the heave direction is between 0.53% and 6.1%. The error comes bigger when KC and ζ increase because the damping forces start to influence every time more. The added mass obtained using ω_n, when KC is less than 0.46, shows a relative error less than 2%, which means the formula based on ω_n gives us a reasonable estimate of the added mass, but for KC 1.52$\leq KC \leq$ 3.43, the error is between 2% and 6%, therefore for those conditions, the added mass must be obtained using ω_d.

Finally, in oceanic and naval engineering, the added mass of a body is usually determined by free vibration tests and using Eq. (7) based on undamped natural frequency ω_n. However, this work suggests the use of the exact form of the equation for the damped natural frequency ω_d of the system, Eq. 5, including the viscous damping effects.

7. ACKNOWLEDGEMENTS

The authors would like to thank the CNPq for the scholarship financial support, the company Veox, and their coworkers for the generous support and let the use of the installations and equipment to develop this work.

8. REFERENCES

Avila, J.P.J., 2008. *Modelagem e identificação de parâmetros hidrodinâmicos de um vehículo robótico submarino*. Ph.D. thesis, Escola Politécnica da Universidade de São Paulo, Departamento de Engenharia Mec^atronica, São Paulo, Brasil.

Avila, J.P.J., Julca, J., Maruyama, N. and Adamowski, J.C., 2005. "Hydrodynamic parameter estimation of an unmanned underwater vehicle". In *Proceedings of the 18th International Congress of Mechanical Engineering - COBEM 2005*. Ouro Preto, Brazil.

Blevins, R.D., 2001. *Flow-Induced Vibration*, Vol. Second edition. Krieger Publishing Company.

Brooks, J.E., 1976. "Added mass of marine propellers in axial translation". Technical report, Naval Ship Research and Development Center Bethesda MD.

Cely, J.S., Saltaren, R., Portilla, G., Yakrangi, O. and Barroso, A.R., 2019. "Experimental and computational methodology for the determination of hydrodynamic coefficients based on free decay test: Application to conception and control of underwater robots". *Sensors*, Vol. 19, No. 17.

Felix, K., 2013. *Free decay testing of a semisubmersible offshore floating platform for wind turbines in model scale*. Ph.D. thesis, University of Kassel, Norwegian.

Hamilton, J., 1997. "Transient tension measurements during mooring deployments". Vol. 1, pp. 134–139.

Hammoud, A., Sahili, J., Madi, M. and Maalouf, E., 2021. "Design and dynamic modeling of rovs: estimating the damping and added mass parameters". *Ocean Engineering*, Vol. 239, p. 109818.

Huamani, R., Florez, P., Nina, W. and Bernedo, L., 2023. *Informe Técnico: Desarrollo de Prototipo Hindrax*. Ph.D. thesis, VEOX, Arequipa, Perú.

Sahili, J., Hamoud, A.E.H. and Jammoul, A., 2018. "Rov design optimization: Effect on stability and drag force". In *2018 6th RSI International Conference on Robotics and Mechatronics (IcRoM)*. pp. 413–417.

Sarpkaya, T., 1986. "Force on a circular cylinder in viscous oscillatory flow at low keulegan—carpenter numbers". *Journal of Fluid Mechanics*, Vol. 165, p. 61–71.

Stelson, T.E. and Mavis, F.T., 1957. "Virtual mass and acceleration in fluids". *Transactions of the American Society of Civil Engineers*, Vol. 122, No. 2870.

Stuart, J. and Woodgate, L., 1955. "Experimental determination of the aerodynamic damping on a vibrating circular cylinder". *The London, Edinburgh, and Dublin Philosophical Magazine and Journal of Science*, Vol. 46, No. 372, pp. 40–46.

Summer, B.M. and Fredsoe, J., 2006. *Hydrodynamics around cylindrical structures*, Vol. 26. World Scientific Publishing Co. Re. Ltd.

White, F.M., 2004. *Fluid Mechanics*. McGraw-Hill.

You, E., Michael, L. and Siong, C.C., 2013. "Added mass computation for control of an open-frame remotely-operated vehicle: Application using wamit and matlab". *Journal of'Marine Science and Technology*, Vol. 22, pp. 1–14.

9. RESPONSIBILITY NOTICE

The authors are solely responsible for the printed material included in this paper.